Imperial College London

Imperial College London

Department of Physics

MSc in Physics with Quantum Dynamics - Self Study Project

The Search for the Electron's Electric Dipole Moment

Author:
Daniel Long

Supervisor:
Prof Michael Tarbutt

Abstract

Symmetry and more precisely CPT symmetry is key property of quantum field theories. To explore these theorem observations of CP and T violating quantities are of great interest. The proposed electric dipole moment of the electron poses an example of such violation and has consequently been of interest and keen experimental pursuit since the 1950s. In this review the symmetry violation of an electron EDM is discussed, as well as the recent experimental approaches towards a sufficiently sensitive measurement, finally there is a brief discussion of the various proposed future experiments.

September 21, 2022

Contents

1. Introduction

For the last ∼50 years Standard Model predictions have been in agreement with experimental observations. However, despite this agreement it is a widely held view that the Standard Model is not a full description of our universe. Instead there are many beyond the Standard Model (BSM) theories which seek to replace the arbitrariness and seeming incompleteness of the Standard Model, in many cases predicting families of particles, so far unobserved due to their extreme energies. One approach to testing these predictions is through particle colliders such as the Large Hadron Collider (LHC), which attempt to probe these extreme regimes, with the latest experiments reaching energies of up to 14 TeV. However, understanding extreme phenomena does not necessarily require experiments to recreate these extreme energies, instead since the 1950s electric dipole moment (EDM) experiments have been pursued, typically operating at less than a few hundred kelvin.

Experimental searches for permanent particle EDMs stem from their inherent violation of parity and time symmetries, violations which may play a role in many currently unexplained phenomena, such as the matter-antimatter imbalance of our universe. An observation of a non-zero particle EDM would not only provide experimental observation of these asymmetries, but it would also provide a key constraint to models of particle physics, potentially presenting the first experimental observation not accounted for in the standard model.

With this context in mind, the recent advances in experimental precision and proposed future experimental advances are of particular significance in the study of fundamental physics. In this review an overview of an electron EDM (eEDM) and its implications for particle physics is presented in section 2, the key theoretical tools used in the discussed eEDM experiments are described in section 3 and finally there is a discussion of the leading experiments from the last 20 years, as well as an introduction to the proposed future experiments are given in section 4.

2. Background

2.1 What is an electric dipole moment

The most general description of an electric dipole moment (EDM) is as the centre of mass of a charge density distribution. This relationship can be expressed as

$$\mathbf{d} = \int_V \rho(\mathbf{r})\mathbf{r}dV \tag{2.1}$$

where the EDM is denoted by $\mathbf{d}$ and the volume V encloses the charge density distribution $\rho(\mathbf{r})$.

For a particle such as an electron one would typically expect this distribution to be symmetric, with a centre of charge at the centre of the object. However, as we will discuss shortly, an asymmetry is predicted in models of particle physics. Such an asymmetry in charge density for particles such as electron can be visualised as an egg-like shape, as shown in figure 2.1.

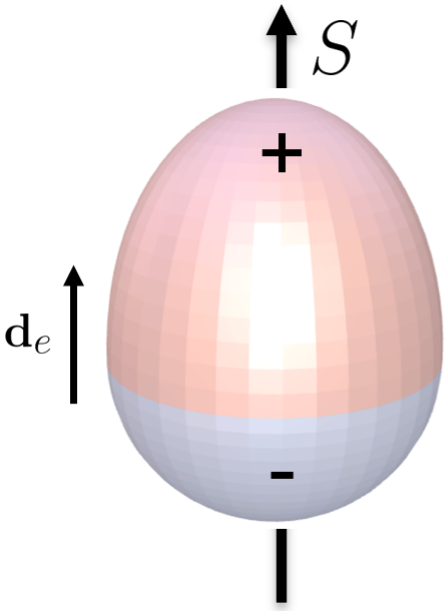

Figure 2.1: Illustration of an asymmetric charge distribution

As the name suggests a key feature of an EDM is the moment on the dipole that results from an applied electric field. For such a dipole the non-relativistic Hamiltonian describing the interaction with an electric field is given by

$$H_d = -\mathbf{d}_e \cdot \mathbf{E}. \tag{2.2}$$

This Hamiltonian will be key to the interferometry used in the subsequently discussed experiments.

2.2 Implications for fundamental theories

There are two major challenges in attempts to explain our universe using the standard model: one is the apparent matter-antimatter imbalance of the universe and the other is apparent observations of dark matter. Many theories have been proposed to account for these unexplained observations, such as the theories of supersymmetry (SUSY) or the Multi-Higgs models, which introduce many symmetry violating particles, so far unobserved. However, before discussing these theories and their predictions, it is worth taking a brief detour in the history of symmetry violation.

2.2.1 CPT Symmetry

Prior to the 1950s it was believed that nature obeyed not only continuous symmetries but also discrete symmetries in charge, parity and time reversal. This view was challenged in 1956, with a review by Yang and Lee noting that whilst parity conservation had been demonstrated experimentally for strong and electromagnetic interactions, it had yet to be shown for weak interactions [1]. Shortly following the publication of this review parity was shown to be violated in the Wu experiment, in which beta decay was found to be favoured in the direction opposite to the nuclear spin [2].

With parity symmetry experimentally violated, it was proposed that a combined charge-parity (CP) symmetry would still hold, however, this too was shown to be violated in the decay of neutral kaons in the 1960s [3]. A proposed symmetry surviving these violations is a combined charge-parity-time (CPT) symmetry, which allows for CP symmetry violation under the requirement of a violation of T symmetry, a violation observed experimentally by the CPLEAR collaboration in 1998 [4].

The connection between the CPT theorem and particle EDMs arises from a particle EDM's inherent parity and time violation. In 1950 Purcell and Ramsay published an early discussion of the possibility for permanent EDMs of elementary particles such as the electron [5]. In this discussion they showed that a non-zero particle EDMs would introduce an inherent violation of parity and time symmetry.

To understand this violation consider a particle with spin $\mathbf{S}$ and an EDM $\mathbf{d}_e$. From the special case of the Wigner-Eckart theorem applied to vector operators, known as the projection theorem, the dipole moment must lie along the axis of $\mathbf{S}$ [6]. A parity transformation would then result in $\mathbf{d}_e \rightarrow -\mathbf{d}_e$, with $\mathbf{S}$ remaining unchanged as $\mathbf{S}$ is pseudovector. On the other hand a time reversal transformation would result in $\mathbf{S} \rightarrow -\mathbf{S}$ and $\mathbf{d}_e$ unchanged. These transformations are illustrated in figure 2.2. In each of the two cases, a change in the relative orientations of the spin and EDM would result in different experimental results therefore creating a violation of parity and time reversal, since these violations occur in both parity and time the CPT theorem holds for particle EDMs.

2.2.2 Theoretical Predictions

Since its development through the latter half of the 20^{th} century, the Standard Model of particle physics has proven highly accurate in its experimental predictions, notably in predictions of quarks, the tau neutrino and most recently the Higgs boson. A criticism however of the Standard Model is the limited CP violation it permits, a phenomenon thought to be a critical mechanism in accounting for phenomenon such as the observed matter-antimatter imbalance of the universe. This limited CP violation leads to the Standard Model predicting an incredibly small eEDM of typically $< 10^{-38}$ e cm [8].

Deviating from the standard model are the various BSM (Beyond Standard Model) theories, such as the family of supersymmetric theories (SUSY). These theories have attempted to resolve issues with the Standard Model such as the hierachy problem[1] via, in the case of supersymmetry, introducing a supersymmetry between bosons and fermions. This supersymmetry leads to a whole scheme of additional of superpartners to Standard Model particles, with the energies of the lightest of which thought to lie a few orders of magnitude above the TeV scale [10]. Whilst many proponents

[1]The hierachy problem addresses the large difference between the scales of various quantities in different fundamental forces, for example the masses of the W and Z particles (the force carriers of the weak force) are 10^{16} times smaller than than the Planck mass (the mass scale of gravity). An introduction to this problem can be found at [9] and a more detailed discussion of application of of supersymmetry to the hierachy problem can be found in [10]

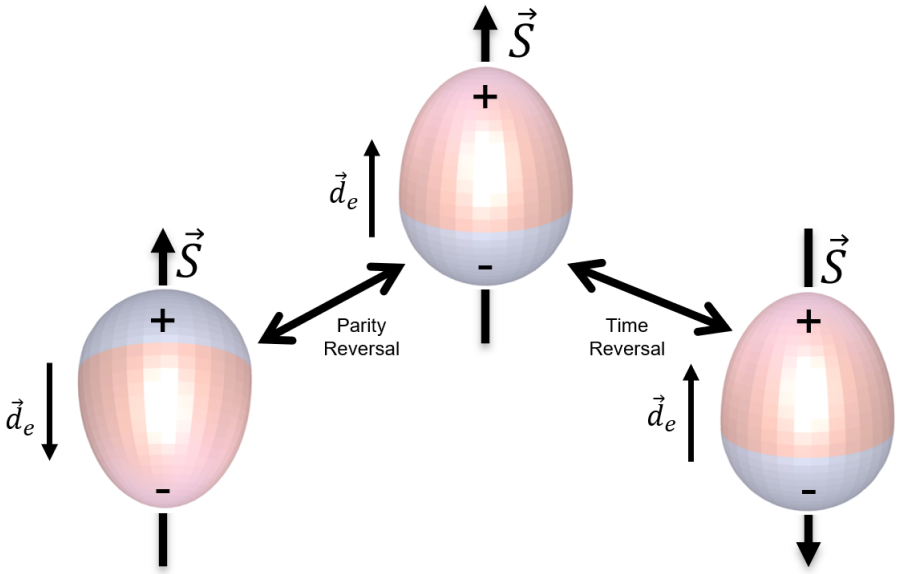

Figure 2.2: Visualisation of the parity and time violation associated with a non-zero particle EDM. On the left a parity reversal transformation is shown, showing a change of sign in the particle's EDM, on the right a time reversal transformation is applied, resulting in the spin being flipped.

of supersymmetry are hopeful of the detection of these superpartners at there LHC, it is proving very challenging to explore these TeV energy scales. An implication of these superpartners is greater CP violation, which relates to eEDM searches as it leads to greater predictions for the magnitude of an eEDM. For a detailed discussion of particle EDMs in supersymmetry please refer to Nakai et al [11].

This observation provides an alternative experimental test for these theories and their predicted superpartners, through measuring a non-zero eEDM with a magnitude greater than the $\sim 10^{-38}$ e cm upper bound of the Standard Model. With the recent progress in eEDM measurements, as well as the potential for significant improvement in the near future, this route is very promising.

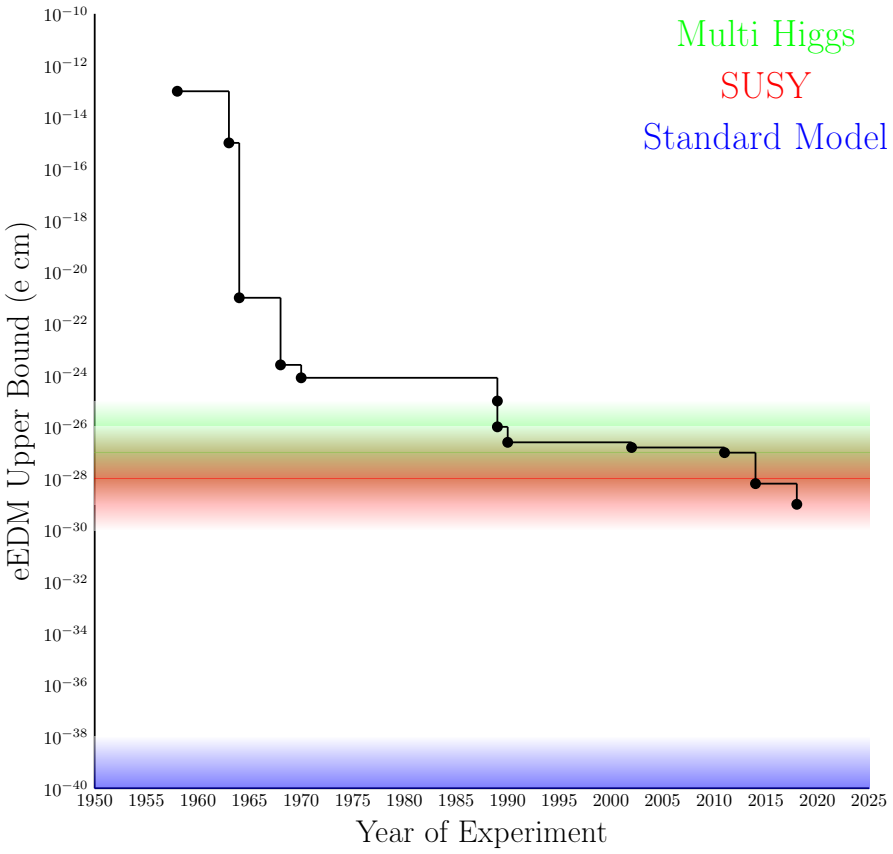

Figure 2.3: A graph of the experimental upper bounds placed on a possible eEDM, with the range of theoretical predictions from the Standard Model and several BSM theories overlayed [7].

3. Key Theoretical Tools

With an appreciation now of the significance of a non-zero eEDM measurement, we can turn our attention to the challenge of achieving such a precise measurement. Possibly the simplest experiment one could devise would be to place an electron in an electric field and measure the energy change of the electron associated with the eEDM interaction, as given in equation 2.2. This approach, whilst simple, falls apart very quickly since a free electron in an electric field will rapidly accelerate, leaving very little time for a precise measurement. A quick calculation shows that with the typical upper limit achievable laboratory electric field of 100kVcm^{-1} and an eEDM of 10^{-29} e cm, the current experimental upper limit, the energy shift associated with an eEDM aligned with the field would be $\sim 10^{-24}$eV. Whilst trying to measure such a small change in energy, the experimenters would have to contend with the electron accelerating at $\sim 10^{18}$m s^{-2}, making this simple approach practically impossible.

Instead experiments have utilised atoms or molecules to confine the electrons (see section 3.1), as well as more sophisticated techniques such as optical pumping (see section 3.3) and carefully tuned fields for achieving specific superposition states (see section 3.4), in order to create interferometers capable of measurements approaching the BSM predicted eEDM. In this section these topics will be reviewed, allowing for a deeper understanding of the modern experiments discussed in section 4.

3.1 Electric Field Enhancement Factor

One major potential issue with measuring the EDM of an electron trapped in an atom is the potential shielding of the atom. Since the atom will polarise in the electric field it will seek a state with zero internal electric field, resulting in no eEDM interaction. This view was first presented in 1963 and is known as Schiff's theorem [12].

Whilst the argument presented by Schiff is valid for a non-relativistic treatment, Sandars showed that the full eEDM interaction term, including relativistic corrections, will evade Schiff's theorem, resulting in a non-zero, or even enhanced eEDM interaction [13]. A detailed explanation for this evasion is given by Commins et al [14], where they show that the evasion arises from a Lorentz contraction of the eEDM in the lab frame.

The evasion and resulting relativistic interaction is typically described by an enhancement factor, R, defined as

$$R = \frac{\mathbf{d}_a}{\mathbf{d}_e}. \tag{3.1}$$

Sandars shows it scales approximately as

$$R \sim PZ^3\alpha^2 \tag{3.2}$$

where P denotes the polarisability of the atom, Z is the atomic number and α is the fine structure constant. This scaling indicates that a greater EDM interaction will be present in heavy atoms.

However, atoms with high atomic numbers also have low polarisabilities, therefore limiting the magnitude of the enhancement. On the other hand molecules show much greater polarisability, allowing them to produce much greater effective electric fields, even in relatively weak applied electric fields.

Due to this significant polarisability the effective electric fields for molecules cannot simply be characterised by a single enhancement factor, instead one needs to consider the form of the

non-linear polarisation of this alignment. Therefore the effective electric field of a molecule is often characterised by the following equation,

$$\mathbf{E}_{eff} = \mathbf{E}_{eff}^{max}\eta(\mathbf{E_{app}})\hat{z} \tag{3.3}$$

where we have chosen the field to be aligned parallel to the z axis. The polarisation factor, denoted by η, ranges from 0 to 1 and describes how the alignment of the molecule changes with respect to the applied field. Since the form of this polarisation factor varies for different molecules it is important to compare their enhancement factors at a specific electric field, in table 3.1 this is chosen to be $E_{app} = 10k\text{Vcm}^{-1}$.

Atom/Molecule	Enhancement Factor, R	Effective Electric Field, E_{eff}	Reference
Caesium, Cs	124	1.2×10^5	[15]
Sodium, Na	0.3	3.3×10^3	[15]
Thallium, Tl	582	5.8×10^5	[15]
Ytterbium Fluoride, YbF	2.6×10^6	2.6×10^{10}	[16]
Thorium Monoxide, ThO	10.4×10^6	10.4×10^{10}	[17]

Table 3.1: Enhancement factors of atoms and molecules previously used or proposed for electron EDM experiments. The molecular enhancement factors and effective electric fields are evaluated at an applied electric field of $E_{app} = 10k\text{Vcm}^{-1}$.

3.2 Atomic energy structure

Atomic energy level structure is key to the atomic beam experimental approach, therefore it is worth providing some background theory on this topic. The entire atomic Hamiltonian, up to hyperfine structure is given in equation (3.4).

$$H = H_0 + V_{Coulomb}\underbrace{-\frac{p^4}{8m^3c^2} + H_{SO} + H_{Darwin}}_{\text{Fine Structure}} + \underbrace{H_{Zeeman}}_{\text{Hyperfine Structure}} + H_{EDM} \tag{3.4}$$

The key interaction in the subsequent atomic beam experiments lies in the hyperfine structure and the EDM interaction. Hyperfine structure arises from electromagnetic multipole moments of the nucleus interacting with the with the magnetic field induced by the orbital motion of the electron and it's spin. When including hyperfine structure the Hamiltonian becomes degenerate unless we consider the diagonal basis of the total spin, F, defined in equation (3.5).

$$\mathbf{F} = \mathbf{I} + \mathbf{J} \tag{3.5}$$

where $\mathbf{I}$ is the nuclear spin and $\mathbf{J}$ is the total angular momentum.

A popular choice of atom for the atomic beam experiment has been Thallium, this is because it is the heaviest stable atom with one valence electron, giving it an enhancement factor of $R \simeq -585$ [18]. The valence electron of Thallium lies in the $6^2P_{1/2}$ ground state, for which $J = 1/2$ and $I = 1/2$, hence the valence electron can take $F = \{0, 1\}$. This implies four different F hyperfine sublevels as the $F = 1$ level has a multiplicity of $2F + 1$.

3.3 Optical Pumping

Optical pumping is a commonly used technique for creating order in the distribution of electronic states in an ensemble of atoms. As the name suggests an optical field, such as a laser, is tuned to pump specific transitions and with specific polarisations it can select for specific sub-levels of the excited state. To determine the probability of these transitions we first define the interaction Hamiltonian to be the dipole interaction between the laser and the atom, given in equation 3.6. Note that we assume the atom and laser are polarised along the z-axis.

$$\hat{H}_{int} = -\hat{\mathbf{d}} \cdot \mathbf{E} = -\hat{d}_z E_z \cos(\omega t) \tag{3.6}$$

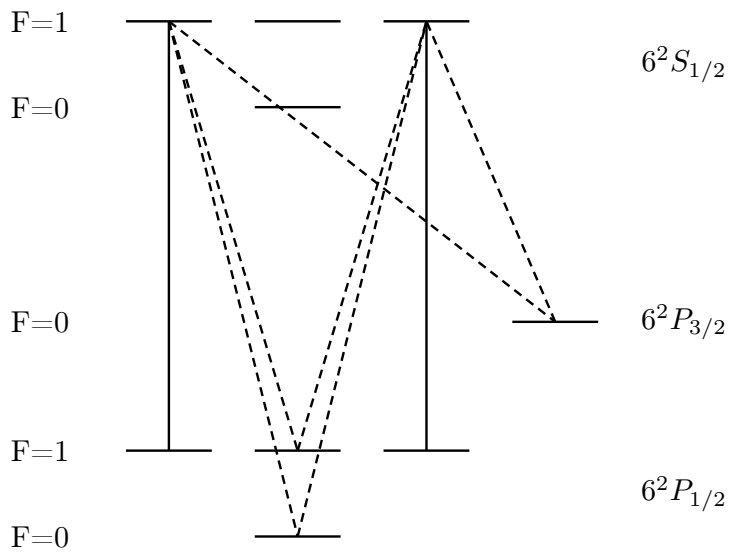

Figure 3.1: Optical pumping of thallium for $m_F = 0$ state selection, driven excitations are denoted by solid lines and spontaneous decays are denoted by dashed lines

The transition probabilities are calculated from the overlap of all possible hyperfine states, this can be performed using the Wigner-Eckhart theorem, as seen in equation 3.7.

$$\langle F', m'_F|\hat{d}_z|F, m_F\rangle = \langle F, m_F, 1, 0|F', m'_F\rangle \langle F'||d||F\rangle \tag{3.7}$$

For the case optical pumping tuned to the $6^2P_{1/2} \rightarrow 6^2S_{1/2}$ transition the Clebsch-Gordon coefficients on the right hand side of equation 3.7 will be non-zero for the excitations shown in solid lines in figure 3.1:

3.4 $\pi/2$ Pulses

The previously discussed state selection process of optical pumping can be used to start the experiment in a pure state. However, often it is a superposition state that is be used to measure interactions between an eEDM and an electric field. Experimentally this superposition state can be achieved by applying a specially tuned pulse, commonly referred to as a $\pi/2$ pulse. To understand this process we start by considering a Hamiltonian of the following form

$$H = H_0 + H_{int} \tag{3.8}$$

where the interaction Hamiltonian H_{int} is defined in equation 3.6.

An arbitrary three level system of states $\{|0\rangle, |1\rangle, |-1\rangle\}$ can be represented in a basis of $\{|0\rangle, |+\rangle, |-\rangle\}$, where we define

$$|+\rangle = \frac{1}{\sqrt{2}}(|1\rangle + |-1\rangle) \tag{3.9}$$

$$|-\rangle = \frac{1}{\sqrt{2}}(|1\rangle - |-1\rangle) \tag{3.10}$$

In this basis our interaction Hamiltonian does not couple the ground state, $|0\rangle$, to the state $|-\rangle$ and therefore in this basis our system is reduced to a two level system. With this reduced two level system one can then follow the approach laid out in Ramsey's book "Molecular Beams" in the derivation of equation V.7 [19], in which the time dependent Schrodinger equation is used, alongside orthogonality constraints, to yield the following propagator associated with the light-atom interaction

$$\Pi_{rf}(t) = \begin{pmatrix} \cos(\omega t)e^{i\frac{\omega}{2}t} & -\sin(\omega t)e^{i\frac{\omega}{2}t} & 0 \\ -\sin(\omega t)e^{-i\frac{\omega}{2}t} & \cos(\omega t)e^{-i\frac{\omega}{2}t} & 0 \\ 0 & 0 & e^{-i\frac{\omega}{2}t} \end{pmatrix} \tag{3.11}$$

where ω is the corresponding angular frequency of the driving field, which is taken to be on resonance with the energy gap between the ground and coherent superposition excited state, $|+\rangle$.

We can understand this propagator more clearly by inspecting two specific timings of the pulse, first lets choose $\omega t = \pi$,

$$\Pi_{rf}(t = \frac{\pi}{\omega}) = \begin{pmatrix} -i & 0 & 0 \\ 0 & i & 0 \\ 0 & 0 & -i \end{pmatrix}. \tag{3.12}$$

This pulse is referred to as a π pulse, assuming the system is initially prepared in the ground state, for example through the optical pumping scheme discussed in the previous section, this pulse will rotate the state around the Bloch sphere, shown in figure 4.2. Another common pulse is defined by $\omega t = \frac{\pi}{2}$, with the corresponding propagator

$$\Pi_{rf}(t = \frac{\pi}{2\omega}) = e^{-i\frac{\pi}{4}} \begin{pmatrix} 0 & i & 0 \\ -1 & 0 & 0 \\ 0 & 0 & 1 \end{pmatrix}. \tag{3.13}$$

For a more detailed discussion of this process, as well as the full propagator, including off resonance driving, please refer to [20].

4. Experimental Approaches

Year	Team	Approach	Upper Limit (e cm)	Reference
1958	Salpeter	Hydrogen Energy Level Splitting	10^{-13}	[21]
1958	Feinberg	Hydrogen Energy Level Splitting	10^{-13}	[22]
1959	Nelson et al.	Spin Precession in a Magnetic Field	10^{-13}	[23]
1963	Goldemberg, Torizuka	Scattering	10^{-15}	[24]
1963	Royce, Bloembergen	Paramagnetic Resonance	1.4×10^{-15}	[25]
1964	Sandars, Lipworth	Atomic Beam	2×10^{-21}	[26]
1968	Weisskopf et al.	Atomic Beam	3×10^{-24}	[27]
1970	Player, Sanders	Atomic Beam	7×10^{-25}	[28]
1989	Cho et al.	Atomic Beam	1.4×10^{-25}	[29]
1989	Murthy et al.	Atomic Beam	1.5×10^{-26}	[30]
1990	Abdullah et al.	Atomic Beam	2.7×10^{-27}	[31]
2002	Regan et al.	Atomic Beam	1.6×10^{-27}	[32]
2011	Hudson et al.	Molecular Beam	1.1×10^{-27}	[33]
2014	ACME	Molecular Beam	8.7×10^{-29}	[34]
2018	ACME	Molecular Beam	1.1×10^{-29}	[35]

Table 4.1: Timeline of the historical the measured upper bounds of the electron's EDM. Since around the 1970s the convention for determining an experimental upper bound has been from the largest possible eEDM that would be viable given a 90% confidence interval on the measured non-zero value.

From table 4.1 it can be seen that from 1964 to 2011 leading experiments have used atomic beams to determine an upper bound on the electron's EDM. These atomic beam experiments attempt to observe an electron's EDM by evolving a carefully selected state (using the techniques outlined in sections 3.2, 3.3 and 3.4). To increase the precision of the measurement the effect is magnified through a large enhancement factor, a concept introduced in section 3.1.

Since 2011 molecular beams have been utilised to further decrease the upper-bound by several orders of magnitude. This improved experimental precision lies predominantly in the the greater enhancement factors of molecules such as ThO and YbF.

In this section the principles of atomic beam experiments will be covered, as well as a subsequent discussion of the more recent molecular beam experiments. Finally there will be a brief introduction to the proposed future experiments, believed to provide even greater precision.

4.1 Shot-Noise Limit

Modern eEDM experiments have typically sought to take a measurement from the energy shift of a molecule due to eEDM interactions. Before exploring the specific approaches of these measurements, it is worth defining the shot-noise limit of a possible eEDM measurement.

We start by defining the EDM induced energy splitting between two states with an opposite parity,

$$\hbar\omega_{EDM} = 2d_e E_{eff} \tag{4.1}$$

where the energy is in the form of an angular frequency. The statistical uncertainty in ω_{EDM} for N independent measurements obeying Poisson statistics is given by

$$T\delta\omega_{EDM} = \frac{1}{\sqrt{N}} \tag{4.2}$$

where T is the interaction duration, for a more detailed explanation please refer to [36].

By combining equations 4.1 and 4.2 we can find the shot-noise limit of the uncertainty in the measured eEDM

$$\delta d_e = \frac{\hbar}{2E_{eff}T\sqrt{N}}. \tag{4.3}$$

From this relation we can see that as a general heuristic longer interaction times, greater effective electric fields and larger ensembles of measurements will result in greater precision on the final measurement. Using this general heuristic, the atomic and molecular beam experiments discussed in this review are compared in table 4.2.

Experiment	E_{eff} (V/cm)	Coherence Time (s)	Population	Shot-noise δd_e (e cm $\sqrt{day}$)	Section	Reference
Tl Beam	7×10^7	2.4×10^{-3}	10^9	2.1×10^{-28}	4.2	[32]
YbF Beam	1.3×10^{10}	10^{-3}	5×10^4	3.8×10^{-28}	4.3.1	[33]
ThO Beam	7.8×10^{10}	10^{-3}	10^5	4.5×10^{-29}	4.3.2	[35]

Table 4.2: Comparison of the shot-noise limit for the discussed experiments.

4.2 Atomic Beam Experiments

In this section we will focus on the atomic beam experiment performed by Regan et al [32]. This experiment is a useful reference as it employed many critical techniques for improving the sensitivity of the experiment, enabling it to achieve the most precise measurement with an atomic beam.

4.2.1 Simplified Experiment

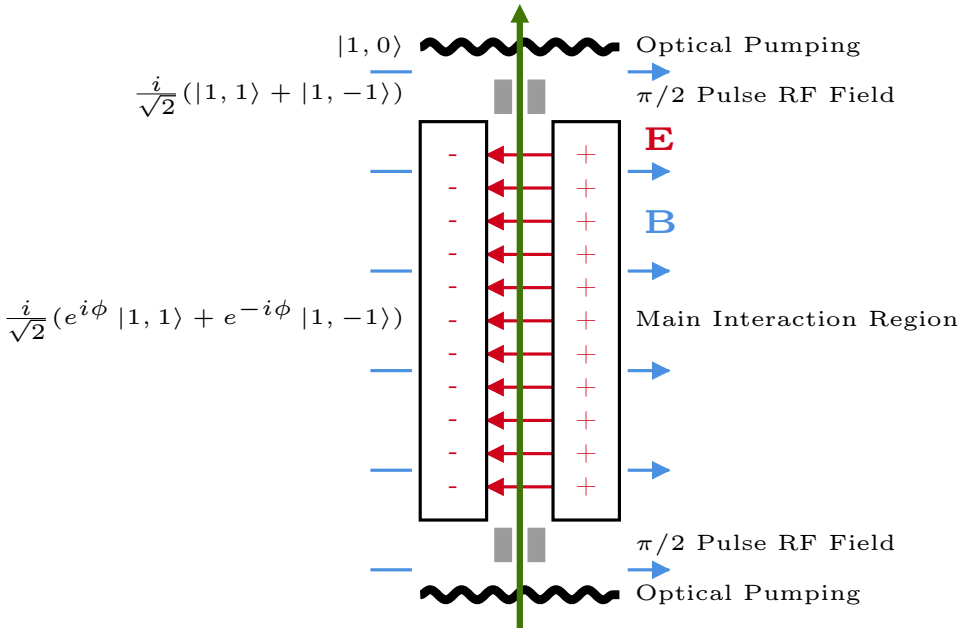

Figure 4.1: Simplified Experimental procedure of the Thallium beam experiment [32]

In figure 4.1 a simplified experimental structure is shown. Mathematically this structure can be understood as the propagator

$$U_{experiment} = U_{pump}U_{\pi/2+\alpha}U_{int}U_{\pi/2}U_{pump}. \tag{4.4}$$

The experiment begins with a region of optical pumping achieved by a laser tuned to 378nm, which excited the $6^2P_{1/2} \rightarrow 6^2S_{1/2}$ transition. As discussed in section 3.3, the probability of excitations can be calculated from the product of the Clebsch-Gordon coefficient and the hyperfine

level coupling, as given in equation 3.7. The Clebsch-Gordon coefficients are only non-zero for excitations from the $m_F = \pm 1$ states, as shown by solid lines in figure 3.1. The decays from these excitations will fall with varying probabilities to the sublevels of the $6^2P_{1/2}$ and $6^2P_{3/2}$ states. It can be found that with a sufficient number of cycles the $|F = 1, m_F = 0\rangle$ sublevel can achieve a population of 34% of the initial flux of atoms, with the remainder of atoms lying in the $6^2P_{3/2}$ or $|F = 0, m_F = 0\rangle$ dark states [37].

Ignoring the dark states we can now consider the wavefunction of the Thallium atoms as

$$|\psi\rangle = |1, 0\rangle \tag{4.5}$$

where our state follows the notation $|F, m_F\rangle$.

The second stage of the experiment was the application of an RF magnetic field, tuned to apply a $\pi/2$ pulse, transforming the Thallium atomic states into a superposition of $m_F = \pm 1$ states. An overview of this process is given in section 3.4 and the motivation for this stage is to prepare the atoms to evolve distinctly in the following main interaction region. The propagator for this process can be written as

$$U_{\pi/2}\,|1, 0\rangle = \frac{i}{\sqrt{2}}(|1, 1\rangle + |1, -1\rangle). \tag{4.6}$$

Once the superposition state is achieved, the thallium atoms enter the main interaction region, which consists of a strong electric field, as well as the background magnetic field. A simplified Hamiltonian, including only dipole interactions, for the atomic states in this region is

$$H = -\boldsymbol{\mu} \cdot \mathbf{B} - \mathbf{d}_e \cdot \mathbf{E}_{eff}. \tag{4.7}$$

The full picture is complicated by higher order features, a discussion of the complete Hamiltonian can be found in [32, 37]. By applying the corresponding propagator for time T the initial superposition state will become

$$\frac{i}{\sqrt{2}} U_{int}(|1, 1\rangle + |1, -1\rangle) = \frac{i}{\sqrt{2}}(e^{i\phi}\,|1, 1\rangle + e^{-i\phi}\,|1, -1\rangle) \tag{4.8}$$

where the phase ϕ is given by

$$\phi = (\boldsymbol{\mu} \cdot \mathbf{B} + \mathbf{d}_e \cdot \mathbf{E}_{eff})\frac{T}{\hbar}. \tag{4.9}$$

This phase can be visualised as a rotation in the x-y plane of the Bloch sphere, as shown in figure 4.2.

After the main interaction region, the Thallium atoms enter another magnetic RF field which applies a $\pi/2$, however in this case there is an additional offset phase, α. The additional phase α will be key to determining the EDM measurement from the signal collected in the subsequent stage. The RF field transforms the thallium atoms with the following propagator

$$U_{\frac{\pi}{2}+\alpha} = \begin{pmatrix} -e^{\frac{i}{2}(\alpha+\frac{\pi}{2})}\sin(\alpha) & -e^{\frac{i}{2}(\alpha+\frac{\pi}{2})}\cos(\alpha) & 0 \\ -\frac{e^{-\frac{i}{2}(\alpha+\frac{\pi}{2})}\cos(\alpha)}{\sqrt{2}} & -\frac{e^{-\frac{i}{2}(\alpha+\frac{\pi}{2})}\sin(\alpha)}{\sqrt{2}} & \frac{e^{-\frac{i}{2}(\alpha+\frac{\pi}{2})}}{\sqrt{2}} \\ -\frac{e^{-\frac{i}{2}(\alpha+\frac{\pi}{2})}\cos(\alpha)}{\sqrt{2}} & -\frac{e^{-\frac{i}{2}(\alpha+\frac{\pi}{2})}\sin(\alpha)}{\sqrt{2}} & -\frac{e^{-\frac{i}{2}(\alpha+\frac{\pi}{2})}}{\sqrt{2}} \end{pmatrix} \tag{4.10}$$

written in the $\{|1, 0\rangle, |1, 1\rangle, |1, -1\rangle\}$ basis. By applying this propagator and then taking the modulus squared we find the probabilities of states $|1, 1\rangle$ and $|1, -1\rangle$ to be

$$P_{|1,1\rangle} = P_{|1,-1\rangle} = \cos^2(\phi)\sin^2(\alpha) + \sin^2(\phi). \tag{4.11}$$

This probability is visualised in figure 4.3. The form of the atomic hyperfine state probability function is key to the final stage of the experiment, which seeks to extract a signal for the phase ϕ. This signal is captured from the fluorescence of decays induced by another region of optical pumping, which follows the same pumping scheme previously discussed and visualised in figure 3.1. The measured count of decays corresponds to the number of excitations, which is dependent on the number of Thallium atoms lying in the $m_F = \pm 1$ states. Therefore by capturing a count of the decays for a range of α configurations, the experimenters were able to determine a measure of $\frac{dP_{|1,\pm1\rangle}}{d\alpha}$, which from figure 4.3 can be seen to be proportional to ϕ. By conducting the experiment with the electric field both parallel and anti-parallel to the magnetic field, the experimenters were able to isolate the evolution corresponding to the eEDM interaction.

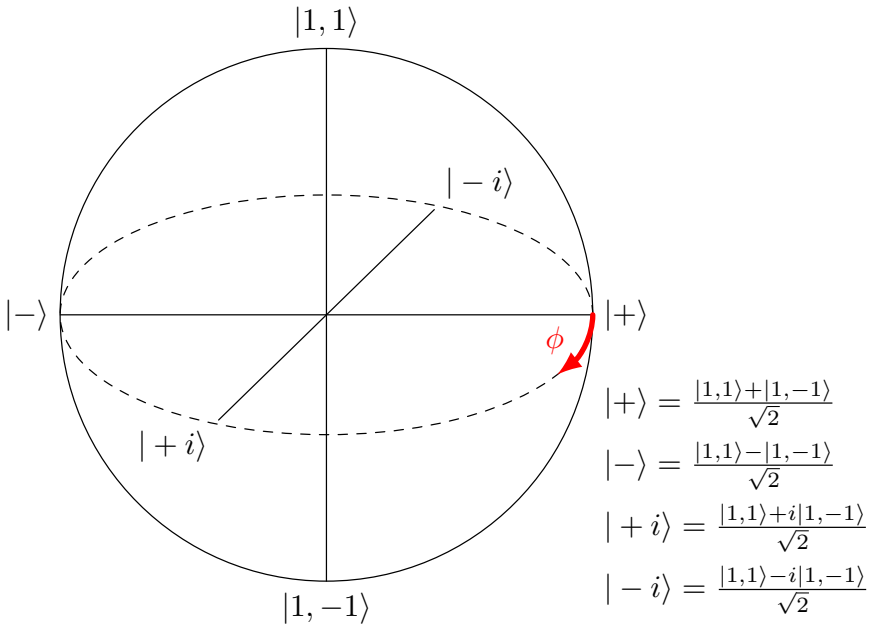

Figure 4.2: Bloch sphere representation for the two level system

4.2.2 Complete Experiment

Whilst the simplified experiment above covers the fundamentals of the experiment, it misses several major subtleties, without which the experiment would be far less accurate. The major source of noise in the experiment is the significant impact of fluctuations in the magnetic field compared to the weak hypothesised eEDM interaction. Several strategies were employed to mitigate this impact, these strategies are be briefly outlined below.

Dual Beam Electric Fields

Instead of conducting the experiment with a single arrangement of electric and magnetic field alignment, the team used a second beam, adjacent to the first, with an opposite electric field direction. This was achieved by using a three electrode configuration, as visualised in figure 4.4. With this configuration the experiment did not require the electric field to be reversed between runs, a process which would introduce systematic errors due to erroneous magnetic fields and other noise.

Sodium Beams

As opposed to attempting to perfectly shield the experiment, the experimenters utilised a control beam of sodium. Sodium is also a para-magnetic atom, however it has a much smaller enhancement factor. Therefore by measuring the magnetic field induced phase shift in sodium, the experimenters were able to in real time subtract the noise in the variation of the magnetic field from the measurement of the thallium phase shift.

Dual Beam Directions

Another source of anomalous magnetic field effects arose from the motion of the atoms. The atomic beams had velocities of the order 10^2ms^{-1}, with significant variation in the velocity distribution. This velocity variation posed a major source of systematic error since for a charge travelling through an electric field an effective magnetic field $\mathbf{B}_{eff}$ is induced, as governed by equation 4.12.

$$\mathbf{B}_{eff} = \frac{1}{c^2}(\mathbf{v} \times \mathbf{E}) \tag{4.12}$$

By using two counter propagating beams on each channel, the experimenters were able to cancel out this induced magnetic field.

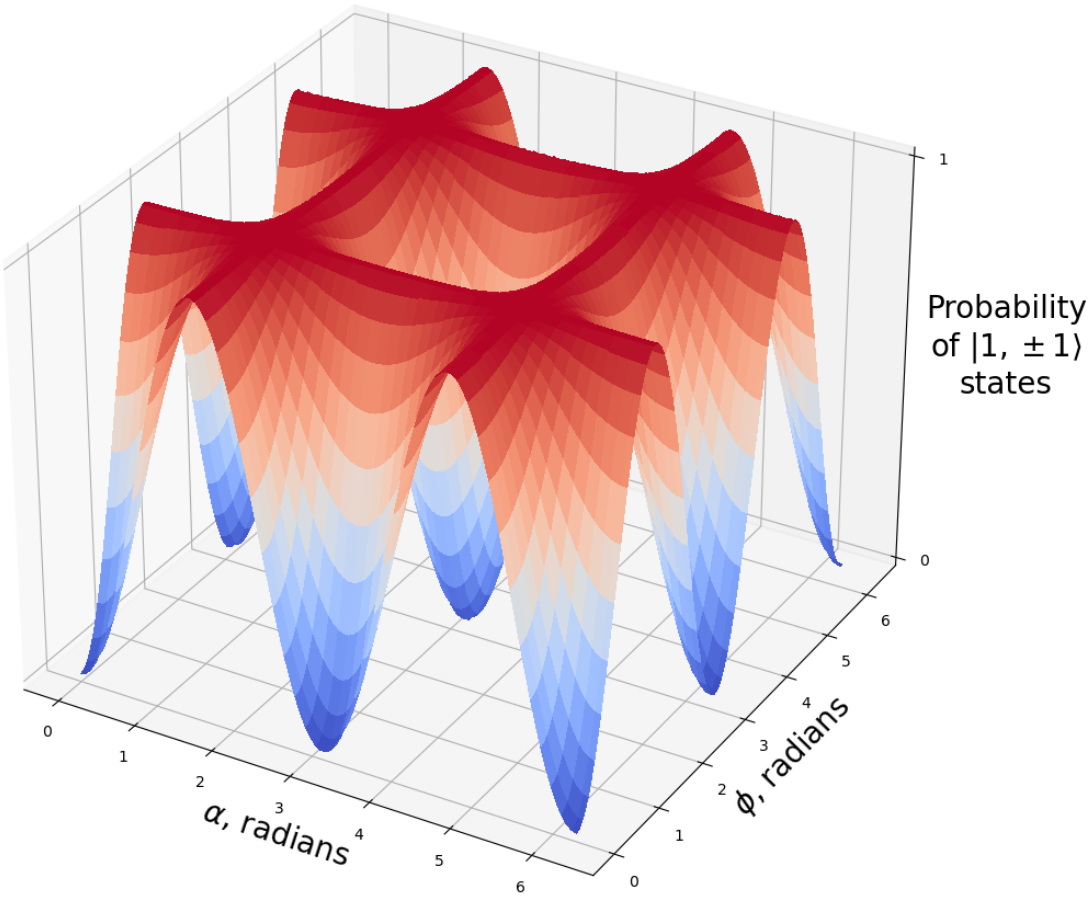

Figure 4.3: Probability of thallium atoms occupying states $|1, \pm 1\rangle$

4.3 Molecular Beams

Since 2011 leading experimental bounds on the electron's EDM have utilised molecular beams of Ytterbium Fluoride (YbF) [33] or Thorium Monoxide (ThO) [34, 35]. The idea of utilising molecular beams is not new, as early as 1967 Sandars presented the case for molecular beams, arguing that their increased polarizability would lead to much greater enhancement factors, and therefore a much more precise experiment [38], a qualitative discussion of the greater enhancement factor is provided in section 3.1. Another motivation for utilising molecular beams is their weaker sensitivity to motional magnetic fields, which were found to be a major limitation in atomic beam experiments. However, despite these benefits these molecules pose major challenges in practice, such as being highly reactive, making them hard to work with in large numbers, as well as having more complex energy level structure, due to the additional internal degrees of freedom present in a molecule relative to an atom.

4.3.1 Ytterbium Fluoride Experiment

Since as early as 2002 eEDM experiments have been conducted using Ytterbium Fluoride [39]. However it was not until 2011 that an experimental upper bound was achieved with a YbF beam. This experiment followed a similar experimental approach to the previously discussed atomic beam experiment (see section 4.2) [40]. The major difference when working with a molecular beam is the vibrational and rotational degrees of freedom. These complications are removed when considering the ground state of YbF. In this state the molecule can be understood as a Yb^2+ core and an F^-

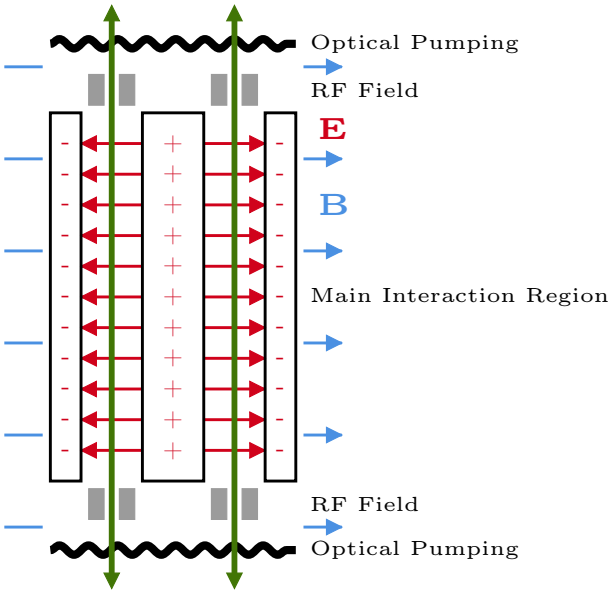

Figure 4.4: Experimental procedure of the Thallium beam experiment [32]

ion with an unpaired valence electron, with the valence electron behaving similarly to an alkali atom's valence electron.

The experiment begins with a regime of optical pumping equivalent to the atomic beam experiment mentioned previously. The ground state of YbF is characterised by two hyperfine level, an $F = 0$ singlet state and an $F = 1$ triplet state. The specific pumping scheme is shown in figure 4.5, and can be seen to mirror the scheme for Thallium, shown in figure 3.1.

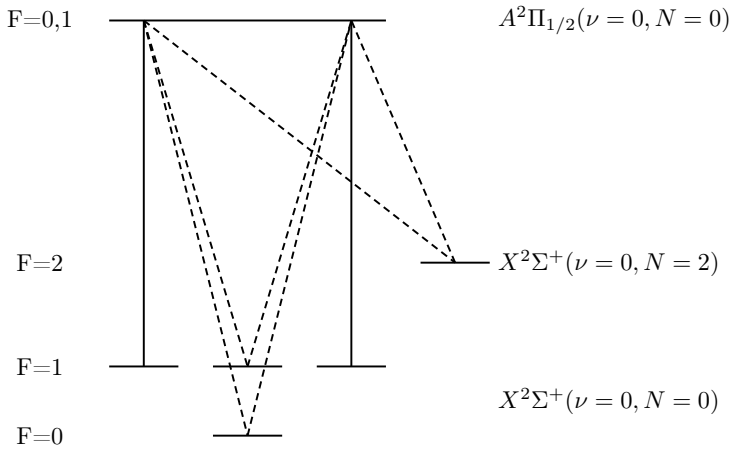

Figure 4.5: Optical pumping of YbF for $m_F = 0$ state selection, driven excitations are denoted by solid lines and spontaneous decays are denoted by dashed lines

Unlike in the Thallium experiment, the YbF molecules then undergo a π pulse in a subsequent RF region. However, despite the experiment using a π instead of a $\pi/2$ pulse, the goal of the pulse was equivalent, producing a superposition state of $m_F = \pm 1$ states. The superposition state then passed through an interaction region where they evolved in an equivalent fashion to the atomic beam case, subject to both a magnetic and electric field.

After the interaction region, the pulses similarly undergo another π pulse which transforms them to a superposition state of $F = 0$ and $F = 1$ states. Finally the population of molecules in the $F = 0$ state is measured by laser induced fluorescence.

Experimental Accuracy and Limitations The major improvement made by the YbF experiment was the greatly reduced sensitivity to magnetic interaction noise relative to the electric

dipole interaction. This reduced sensitivity resulted from the much greater effective electric fields achievable with YbF, as seen in table 3.1.

A much greater relative electric field not only made the EDM interaction much greater, but it also had secondary effects which further reduced noise. Previously we discussed the application of dual beam directions in the Thallium beam experiment, so as to cancel the effective magnetic fields induced by the velocities of the atoms. It turns out that this effect is inherently reduced for the YbF experiment. Due to the increased polarisability of the molecule, and therefore its much greater alignment to the electric field direction (which is parallel to the magnetic field), the motional magnetic field effects, which arises from a magnetic field perpendicular to the electric field are greatly suppressed. This systematic effect was the major limiting factor of previous EDM experiments, hence this development explains much of the improved sensitivity, an improvement not apparent in the simple shot-noise limits in table 4.2.

4.3.2 Thorium Monoxide Experiment

Molecular beam searches for a non-zero eEDM have not been restricted to YbF, instead many other molecules have been explored, notably in early experiments using lead oxide (PbO) and more recent experiments using thorium monoxide (ThO). These experiments were motivated by the convenient Ω-doublet states found in both molecules, which would allow for greater sensitivity and reduction of systematic effects.

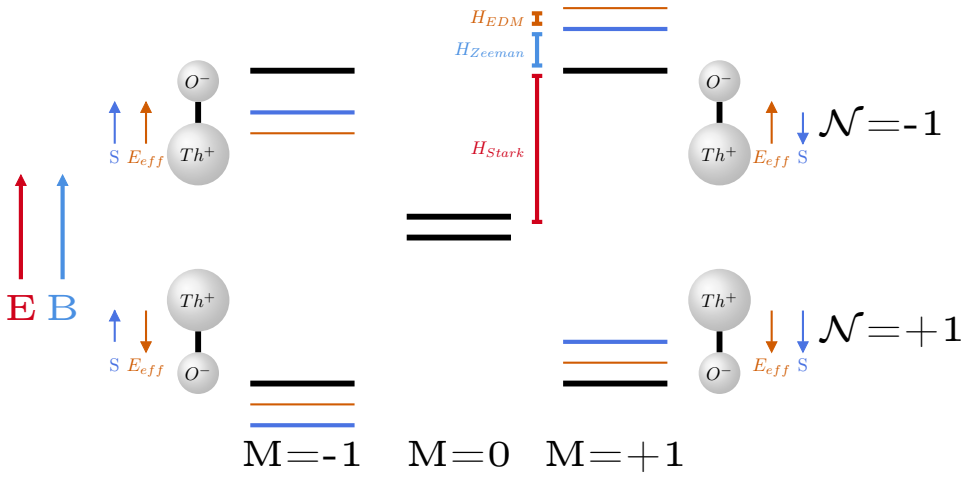

Figure 4.6: An energy level diagram for the ThO H state in external magnetic and electric fields, showing an example of Ω doublets. The molecule undergoes Stark, Zeeman and EDM interaction energy shifts, where the relative signs of the energy shifts are given by: sign(H_{Stark}) = M, sign(H_{Zeeman}) = -$\mathcal{N}$ and sign(H_{EDM}) = -$M\mathcal{N}$. It can be seen that the relative signs of the EDM and Zeeman interactions can be reversed by only considering specific polarisation states, without any need to change the applied fields.

Before discussing the individual experiments, it is worth providing a brief overview of Ω-doublets and their application in eEDM experiments. Ω-doublets are closely spaced states of opposite polarisation parity, this means that the internal electric field of these states are defined by the parity of the state. A detailed discussion of these states can be found in [36], however for this discussion the key properties to note are the:

Field Independent eEDM Shift Reversal Depending on the orientation of the polar molecule with respect to parallel electric and magnetic fields the relative direction of the Zeeman and EDM energy shifts will differ, as seen in figure 4.6. This allows the Zeeman energy shift to be cancelled by subtracting the quantum beat frequencies of the two orientations. Quantum beats are the decay fluorescence interference patterns resulting from a superposition of non-zero spin projection states ($m \neq 0$) decaying onto an $m = 0$ state and interfering with each other due to a phase difference. In practice this process is more complex as one has to account for the Stark shift, a more detailed discussion of this effect can be found in [41]. In figure 4.7 an example of this application of Ω-doublets can be seen.

Greater Enhancement Factor Ω-doublets also contribute to the previously mentioned large enhancement factor which allows the experiment to be performed with a modest electric field. By not needing to maximise the electric field many systematic effects associated with this field and the correlated magnetic fields produced by leakage currents can be avoided.

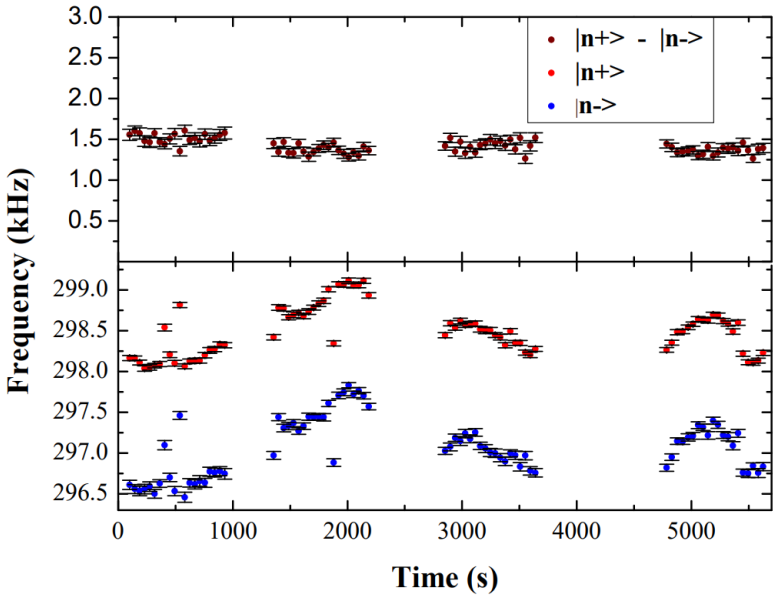

Figure 4.7: An example of the application of an Ω-doublet in the cancelling of magnetic field fluctuation. Below the individual state florescence signals are shown and on top the florescence signals are subtracted, figure reproduced from [41].

In 2001 DeMille et al first proposed using PbO, the motivation for its use was the possibility of conducting the experiment in a vapor cell, allowing for much higher densities than in the traditional beam approach, as well as the discussed reduction in systematic effects through use of Ω-doublet field reversal [42]. However, despite these advantages, in practice complications arising from electric and magnetic field gradients led to additional systematic effects, resulting in a less sensitive measurement than the previous YbF experiment [43].

More recently DeMille and the ACME (Advanced Cold Molecule Electron) collaboration have switched to using ThO, owing to its Ω-doublet state, its greater enhancement factor, as well as other useful properties, such as its relatively stable ground state and its amenability to expansion cooling, allowing for a low velocity, high flux beam. Since 2014 the ACME collaboration has measured the leading experimental upper bounds on the eEDM. These measurements used ThO in a similar beam approach to the earlier YbF experiment (see section 4.3.1) and the preceding atomic beam experiments (see section 4.2).

The main difference from previous experiments and the ACME 2014 measurement [34] was incorporating Ω-doublet parity state selection into the optical pumping scheme. Since the Ω-doublet states are split by a significant Stark shift, as indicated in figure 4.6, the detuned Ω-doublet state will be a dark state and will act as the initial state of the experiment. This experiment achieved an order of magnitude smaller upper limit on the eEDM, placing the limit at 8.7×10^{-29} e cm.

In 2018 the ACME collaboration improved on this limit by increasing the flux of ThO molecules usable in the measurement. The previous approach of state selection via optical pumping achieved an efficiency of approximately 6%. Through employing a Stimulated Raman Adiabatic Passage (STIRAP) process the experiment managed to reach efficiencies of $75\% \pm 5\%$ [44]. STIRAP allows for two states of a three level system to be coupled via a third intermediate state, whilst also not populating the intermediate state. By not populating this intermediate state the process becomes more efficient as there will not be spontaneous emission (potentially to dark states) from this intermediate state. For a comprehensive overview of STIRAP please refer to [45].

With this improvement in the beam flux, as well as other enhancements from improved experimental geometry and fluorescence detection, the team were able to achieve another order of

improvement on the eEDM upper limit, measuring a limit of 1.1×10^{-29} e cm

4.3.3 Trapped Ion Experiment

A more distinct approach pursued by Cairncross et al was using trapped ions. The ions are trapped with an oscillating RF field, sometimes referred to as a Paul trap, . The ions are trapped due to the field which increases in strength radially from the centre of the trap, the field oscillates with a frequency in resonance with the motion of the ions. As the ions move further from the centre of the trap in one dimension they experience a large restoring force due to the field. Whilst the ions then cross the centre of the trap in that dimension, the field is applied in an orthogonal dimension applying a restoring force in the orthogonal dimension. Whilst the ions travel through the centre the field in the initial dimension is weak, resulting in less force and the ions biased towards the centre of the trap.

In 2017 Cairncross et al used HfF^+ ions in an RF trap to achieve spin-precession times of over 700 ms [46]. Whilst in the trap, the ions underwent an equivalent scheme to the previous beam experiments, apart from utilising an Ω-doublet structure, as in the ThO experiment, to negate the need for a reversal of the applied electric field and therefore reducing potential systematic errors. This experiment found an upper bound on the eEDM of 9.4×10^{-29} e cm, slightly higher than the result achieved by the ThO experiment [35], however notable for confirming a zero value via a different approach.

4.4 Future Experiments

The heuristic from section 4.1 not only helps analyse the relative advantages and limitations of past experiments, as in table 4.2, but also assists the analysis of proposed future experiments, which seek to advance the current experimental upper bound to sensitivities of over 10^{-32} e cm.

4.4.1 Ultracold Molecule Experiments

The current leading upper bound from the ACME II experiment makes use of both a high internal electric field and a high flux molecular beam, however the spin precession time is limited by the coherence time of the chosen state, which is of the order of milliseconds [36]. One proposed remedy for this limitation is using ultracold molecules to increase the coherence time of the spin-precession state. In recent years it has been shown that molecules can be laser cooled as low as $5\mu K$ [47], leading many research teams to explore applying these advances to eEDM experiments, for example there are teams working with YbF [48], YbOH [49] and with BaF [50].

The scale of this improvement can be gauged from the resulting shot-noise limit with the proposed coherence times. For example, Fitch et al gave a conservative estimate for the coherence time of an ultracold YbF beam of 100 ms, resulting in a shot-noise limited upper bound of 1.1×10^{-31} per $\sqrt{\text{day}}$, two orders of magnitude smaller than the currently measured eEDM upper bond [51].

4.4.2 Optical Lattice Experiments

Building on the planned ultracold molecular beam experiment, the team at Imperial have proposed future experiments using a 3D optical lattice trap. This experiment would once again follow a similar approach to the molecular beam experiments, however the molecules would be loaded into a 3D trap consisting of two electrodes and three orthogonal pairs of counter-propagating red-detuned lasers. The trap operates by first trapping the molecules with velocity dependent scattering of the Doppler shifted red-detuned lasers and magnetic field damping due to the two coils. The trapped molecules then behave as if in a damped harmonic oscillator. Additionally, the molecules are further cooled beyond the Doppler limit due to Sisyphus cooling, arising from the counter-propagation of the lasers.

Given that the coherence time of the molecule's spin precession is limited by the scattering rate of the optical trap and the collision rate with the background gas, which can both be reduced to below $0.1s^{-1}$, the molecules could reach coherence times of around 10 seconds. This could then yield a shot-noise limited uncertainty of as low as 2×10^{-32} e cm per $\sqrt{\text{day}}$ [51].

4.4.3 Solid State Lattice Experiments

So far the discussed future experiments have focused on improving the current upper bond by increasing the coherence time of the experiment. However another route is via increasing the number of molecules measured, as seen in equation 4.3. A collaboration of researchers from York University, Michigan State University and the University of Toronto have proposed embedding polar molecules in an inert-gas matrix, in an approach they refer to as EDM^3.

The team has argued that it should be possible to achieve coherence times of 1 second, with numbers of embedded molecules of up to 10^16. With this in mind, they propose that they could reach many orders of magnitude lower than the current upper bound, with a month long measurement achieving a shot-noise limited uncertainty of $10^{-35} \sim 10^{-37}$ e cm [52].

4.4.4 Polyatomic Molecule Experiments

Laser cooling of polyatomic molecules is a relatively recent advance, with a recent demonstration in 2017 by Kozyryev et al showing laser cooling of strontium monohydroxide (SrOH) down to $\sim$750μK [53]. This work has been in part motivated by the possibility of applying laser cooled polyatomic molecules to eEDM measurements [49]. Polyatomic molecules are seen as amenable to a precise measurement due to their low lying vibrational states which offer full polarisation, as well as the possibility of co-magnetometry analogous to the previously discussed Ω-doublet structure. The possibility of co-magnetometry in polyatomic molecules arises from degenerate bending vibrational modes. As with Ω-doublet states the polarisation of the molecule determines the sign of the Stark shift, however the EDM shift is determined by the projection of the modes angular momentum, an independent property, allowing for co-magnetometry.

Through the laser cooling and trapping the molecules in a MOT Kozyryev et al argue that they could reach populations of 10^6, with coherence times of up to 10 seconds. With these advantages, alongside the high internal electric fields of such molecules, the team proposes a shot noise limited measurement up to four orders of magnitude more precise than the current upper bound.

Bibliography

[1] T. D. Lee and C. N. Yang. Question of parity conservation in weak interactions. *Phys. Rev.*, 104:254–258, Oct 1956.

[2] C. S. Wu, E. Ambler, R. W. Hayward, D. D. Hoppes, and R. P. Hudson. Experimental test of parity conservation in beta decay. *Phys. Rev.*, 105:1413–1415, Feb 1957.

[3] J. H. Christenson, J. W. Cronin, V. L. Fitch, and R. Turlay. Evidence for the 2π decay of the k_2^0 meson. *Phys. Rev. Lett.*, 13:138–140, Jul 1964.

[4] A. Angelopoulos, A. Apostolakis, E. Aslanides, G. Backenstoss, P. Bargassa, O. Behnke, A. Benelli, V. Bertin, F. Blanc, P. Bloch, P. Carlson, M. Carroll, E. Cawley, S. Charalambous, M.B. Chertok, M. Danielsson, M. Dejardin, J. Derre, A. Ealet, C. Eleftheriadis, L. Faravel, W. Fetscher, M. Fidecaro, A. Filipčič, D. Francis, J. Fry, E. Gabathuler, R. Gamet, H.-J. Gerber, A. Go, A. Haselden, P.J. Hayman, F. Henry-Couannier, R.W. Hollander, K. Jon-And, P.-R. Kettle, P. Kokkas, R. Kreuger, R. Le Gac, F. Leimgruber, I. Mandić, N. Manthos, G. Marel, M. Mikuž, J. Miller, F. Montanet, A. Muller, T. Nakada, B. Pagels, I. Papadopoulos, P. Pavlopoulos, A. Policarpo, G. Polivka, R. Rickenbach, B.L. Roberts, T. Ruf, C. Santoni, M. Schäfer, L.A. Schaller, T. Schietinger, A. Schopper, L. Tauscher, C. Thibault, F. Touchard, C. Touramanis, C.W.E. Van Eijk, S. Vlachos, P. Weber, O. Wigger, M. Wolter, D. Zavrtanik, and D. Zimmerman. First direct observation of time-reversal non-invariance in the neutral-kaon system. *Physics Letters B*, 444(1):43–51, 1998.

[5] E. M. Purcell and N. F. Ramsey. On the possibility of electric dipole moments for elementary particles and nuclei. *Phys. Rev.*, 78:807–807, Jun 1950.

[6] J.J. Sakurai. *Modern Quantum Mechanics*, page 238–242. Addison-Wesley, 1994.

[7] J.M. Pendlebury and E.A. Hinds. Particle electric dipole moments. *Nuclear Instruments and Methods in Physics Research Section A: Accelerators, Spectrometers, Detectors and Associated Equipment*, 440(3):471–478, 2000.

[8] Maxim Pospelov and Adam Ritz. Electric dipole moments as probes of new physics. *Annals of physics*, 318(1):119–169, 2005.

[9] Matt Strassler. The hierarchy problem, 2011. `https://profmattstrassler.com/articles-and-posts/particle-physics-basics/the-hierarchy-problem/`.

[10] Stephen P. Martin. A supersymmetry primer. *Advanced Series on Directions in High Energy Physics*, page 1–98, Jul 1998.

[11] Yuichiro Nakai and Matthew Reece. Electric dipole moments in natural supersymmetry. *Journal of High Energy Physics*, 2017(8), Aug 2017.

[12] L. I. Schiff. Measurability of nuclear electric dipole moments. *Phys. Rev.*, 132:2194–2200, Dec 1963.

[13] P.G.H Sandars. The electric dipole moment of an atom. *Physics letters*, 14(3):194–196, 1965.

[14] J.D. Jackson E.D. Commins and D.P. DeMille. The electric dipole moment of an atom. *American Journal of Physics*, 75:532–536, 2007.

[15] V. A. Dzuba and V. V. Flambaum. Calculation of the (t, p)-odd electric dipole moment of thallium and cesium. *Phys. Rev. A*, 80:062509, Dec 2009.

[16] N S Mosyagin, M G Kozlov, and A V Titov. Electric dipole moment of the electron in the ybf molecule. *Journal of Physics B: Atomic, Molecular and Optical Physics*, 31(19):L763–L767, Oct 1998.

[17] Edmund R. Meyer and John L. Bohn. Prospects for an electron electric-dipole moment search in metastable tho andthf+. *Physical Review A*, 78(1), Jul 2008.

[18] Z. W. Liu and Hugh P. Kelly. Analysis of atomic electric dipole moment in thallium by all-order calculations in many-body perturbation theory. *Phys. Rev. A*, 45:R4210–R4213, Apr 1992.

[19] Norman F. Ramsey. *Molecular beams.* International series of monographs on physics. Clarendon P, 1956.

[20] MR Tarbutt, JJ Hudson, BE Sauer, and EA Hinds. Preparation and manipulation of molecules for fundamental physics tests. pages 555–596, 2009.

[21] E. E. Salpeter. Some atomic effects of an electronic electric dipole moment. *Phys. Rev.*, 112:1642–1648, Dec 1958.

[22] G. Feinberg. Effects of an electric dipole moment of the electron on the hydrogen energy levels. *Phys. Rev.*, 112:1637–1642, Dec 1958.

[23] D. F. Nelson, A. A. Schupp, R. W. Pidd, and H. R. Crane. Search for an electric dipole moment of the electron. *Phys. Rev. Lett.*, 2:492–495, Jun 1959.

[24] J. Goldemberg and Y. Torizuka. Upper limit of the electric dipole moment of the electron. *Phys. Rev.*, 129:2580–2581, Mar 1963.

[25] E. B. Royce and N. Bloembergen. Linear electric shifts in the paramagnetic resonance of al_2o_3: Cr and mgo: Cr. *Phys. Rev.*, 131:1912–1923, Sep 1963.

[26] P. G. H. Sandars and E. Lipworth. Electric dipole moment of the cesium atom. a new upper limit to the electric dipole moment of the free electron. *Phys. Rev. Lett.*, 13:718–720, Dec 1964.

[27] M. C. Weisskopf, J. P. Carrico, H. Gould, E. Lipworth, and T. S. Stein. Electric dipole moment of the cesium atom. a new upper limit to the electric dipole moment of the electron. *Phys. Rev. Lett.*, 21:1645–1648, Dec 1968.

[28] M A Player and P G H Sandars. An experiment to search for an electric dipole moment in the3p2metastable state of xenon. *Journal of Physics B: Atomic and Molecular Physics*, 3(12):1620–1635, dec 1970.

[29] D. Cho, K. Sangster, and E. A. Hinds. Tenfold improvement of limits on t violation in thallium fluoride. *Phys. Rev. Lett.*, 63:2559–2562, Dec 1989.

[30] S. A. Murthy, D. Krause, Z. L. Li, and L. R. Hunter. New limits on the electron electric dipole moment from cesium. *Phys. Rev. Lett.*, 63:965–968, Aug 1989.

[31] K. Abdullah, C. Carlberg, E. D. Commins, Harvey Gould, and Stephen B. Ross. New experimental limit on the electron electric dipole moment. *Phys. Rev. Lett.*, 65:2347–2350, Nov 1990.

[32] B. C. Regan, Eugene D. Commins, Christian J. Schmidt, and David DeMille. New limit on the electron electric dipole moment. *Phys. Rev. Lett.*, 88:071805, Feb 2002.

[33] I.J. Smallman B.E. Sauer M.R. Tarbutt J.J. Hudson, D.M. Kara and E.A. Hinds. Upper limit of the electric dipole moment of the electron. *Nature*, 473:493–496, 2011.

[34] ACME Collaboration. Order of magnitude smaller limit on the electric dipole moment of the electron. *Science*, 343:269–272, 2014.

[35] ACME Collaboration. Improved limit on the electric dipole moment of the electron. *Nature*, 562:355–360, 2018.

[36] A C Vutha, W C Campbell, Y V Gurevich, N R Hutzler, M Parsons, D Patterson, E Petrik, B Spaun, J M Doyle, G Gabrielse, and D DeMille. Search for the electric dipole moment of the electron with thorium monoxide. *Journal of Physics B: Atomic, Molecular and Optical Physics*, 43(7):074007, Mar 2010.

[37] Brian C. Regan. *A search for violation of time -reversal symmetry in atomic thallium*. PhD thesis, 2001. Copyright - Database copyright ProQuest LLC; ProQuest does not claim copyright in the individual underlying works; Last updated - 2021-05-22.

[38] P. G. H. Sandars. Measurability of the proton electric dipole moment. *Phys. Rev. Lett.*, 19:1396–1398, Dec 1967.

[39] J. J. Hudson, B. E. Sauer, M. R. Tarbutt, and E. A. Hinds. Measurement of the electron electric dipole moment using ybf molecules. *Phys. Rev. Lett.*, 89:023003, Jun 2002.

[40] J.J. Hudson B.E. Sauer M.R. Tarbutt D.M. Kara, I.J. Smallman and E.A. Hinds. Measurement of the electron's electric dipole moment using YbF molecules: methods and data analysis. *New Journal of Physics*, 14(10):103051, oct 2012.

[41] Paul Hamilton. Preliminary results in the search for the electron electric dipole moment in lead oxide. 01 2010.

[42] D. DeMille, F. Bay, S. Bickman, D. Kawall, L. Hunter, D. Krause, S. Maxwell, and K. Ulmer. Search for the electric dipole moment of the electron using metastable pbo. *AIP Conference Proceedings*, 596(1):72–83, 2001.

[43] S. Eckel, P. Hamilton, E. Kirilov, H. W. Smith, and D. DeMille. Search for the electron electric dipole moment using-doublet levels in pbo. *Physical Review A*, 87(5), May 2013.

[44] C. D. Panda, B. R. O'Leary, A. D. West, J. Baron, P. W. Hess, C. Hoffman, E. Kirilov, C. B. Overstreet, E. P. West, D. DeMille, J. M. Doyle, and G. Gabrielse. Stimulated raman adiabatic passage preparation of a coherent superposition of tho $H^3\Delta_1$ states for an improved electron electric-dipole-moment measurement. *Phys. Rev. A*, 93:052110, May 2016.

[45] Nikolay V. Vitanov, Andon A. Rangelov, Bruce W. Shore, and Klaas Bergmann. Stimulated raman adiabatic passage in physics, chemistry, and beyond. *Reviews of Modern Physics*, 89(1), Mar 2017.

[46] William B. Cairncross, Daniel N. Gresh, Matt Grau, Kevin C. Cossel, Tanya S. Roussy, Yiqi Ni, Yan Zhou, Jun Ye, and Eric A. Cornell. Precision measurement of the electron's electric dipole moment using trapped molecular ions. *Phys. Rev. Lett.*, 119:153001, Oct 2017.

[47] L. Caldwell, J. A. Devlin, H. J. Williams, N. J. Fitch, E. A. Hinds, B. E. Sauer, and M. R. Tarbutt. Deep laser cooling and efficient magnetic compression of molecules. *Phys. Rev. Lett.*, 123:033202, Jul 2019.

[48] M R Tarbutt, B E Sauer, J J Hudson, and E A Hinds. Design for a fountain of YbF molecules to measure the electron's electric dipole moment. *New Journal of Physics*, 15(5):053034, may 2013.

[49] Ivan Kozyryev and Nicholas R. Hutzler. Precision measurement of time-reversal symmetry violation with laser-cooled polyatomic molecules. *Phys. Rev. Lett.*, 119:133002, Sep 2017.

[50] The NL eEDM collaboration. Measuring the electric dipole moment of the electron in baf. *The European Physical Journal D*, 72, Nov 2018.

[51] N J Fitch, J Lim, E A Hinds, B E Sauer, and M R Tarbutt. Methods for measuring the electron's electric dipole moment using ultracold YbF molecules. *Quantum Science and Technology*, 6(1):014006, Dec 2020.

[52] A. Vutha, M. Horbatsch, and E. Hessels. Oriented polar molecules in a solid inert-gas matrix: A proposed method for measuring the electric dipole moment of the electron. *Atoms*, 6(1):3, Jan 2018.

[53] Ivan Kozyryev, Louis Baum, Kyle Matsuda, Benjamin L. Augenbraun, Loic Anderegg, Alexander P. Sedlack, and John M. Doyle. Sisyphus laser cooling of a polyatomic molecule. *Phys. Rev. Lett.*, 118:173201, Apr 2017.